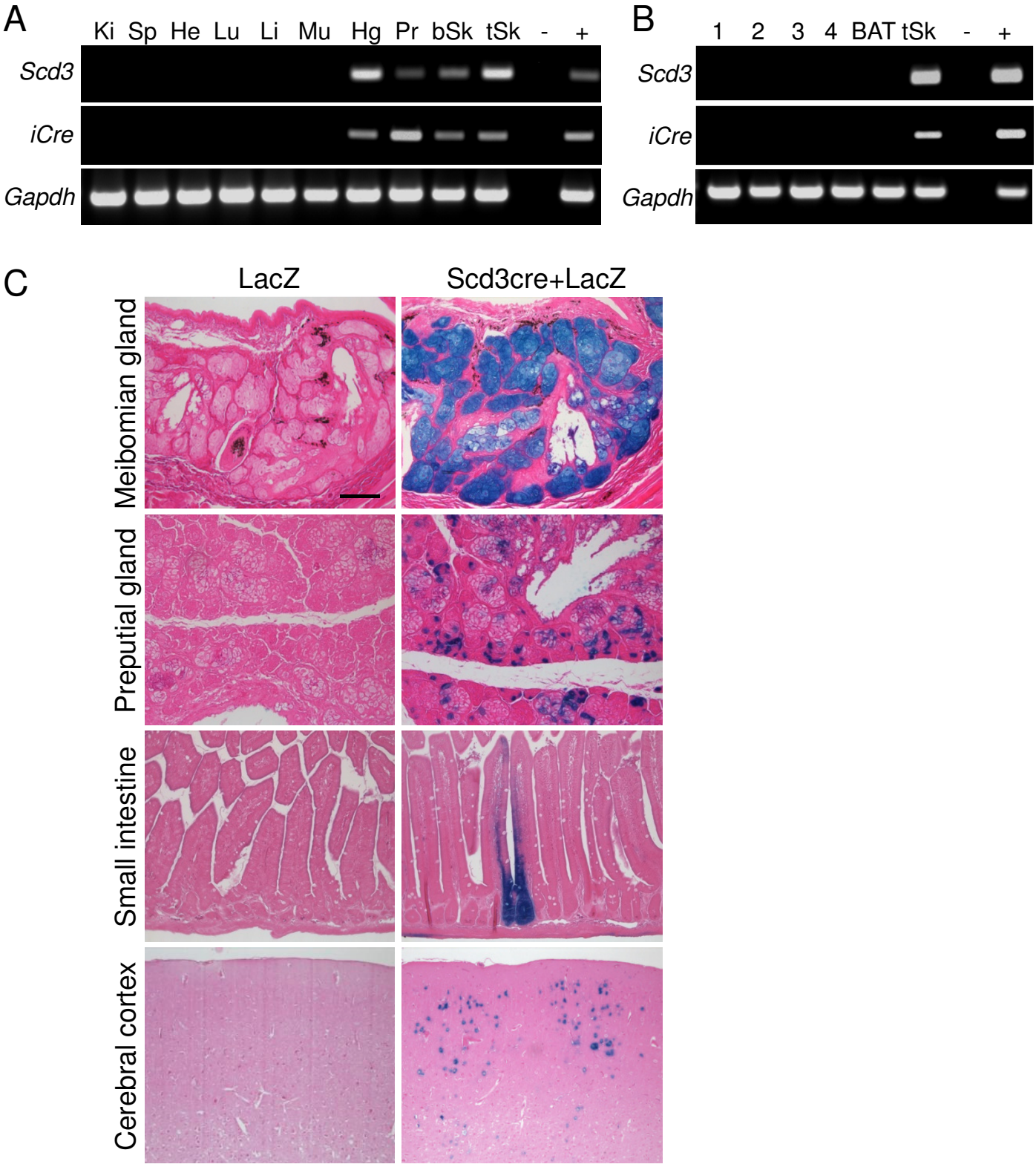

Fig. S1. Expression of cre under the control of the *Scd3* locus. (A) RT-PCR analysis confirmed that expression of *Scd3* and *iCre* was limited to back (bSk) and tail (tSk) skin and to the Harderian (Hg) and preputial (Pr) glands. Ki, kidney; Sp, spleen; He, heart; Lu, lung; L, liver; Mu, muscle. (B) RT-PCR analysis also confirmed that *Scd3* and *iCre* are not expressed in the subcutaneous (1), perirenal (2), abdominopelvical (3), and perigonadal (4) white adipose tissue depots or in brown adipose tissue (BAT). (C) Staining for β-galactosidase activity revealed expression of cre in Meibomian and preputial glands, in a small number of cells in the small intestinal epithelium, and in a few neurons in the cerebral cortex. Scale bar indicates 50 μm.

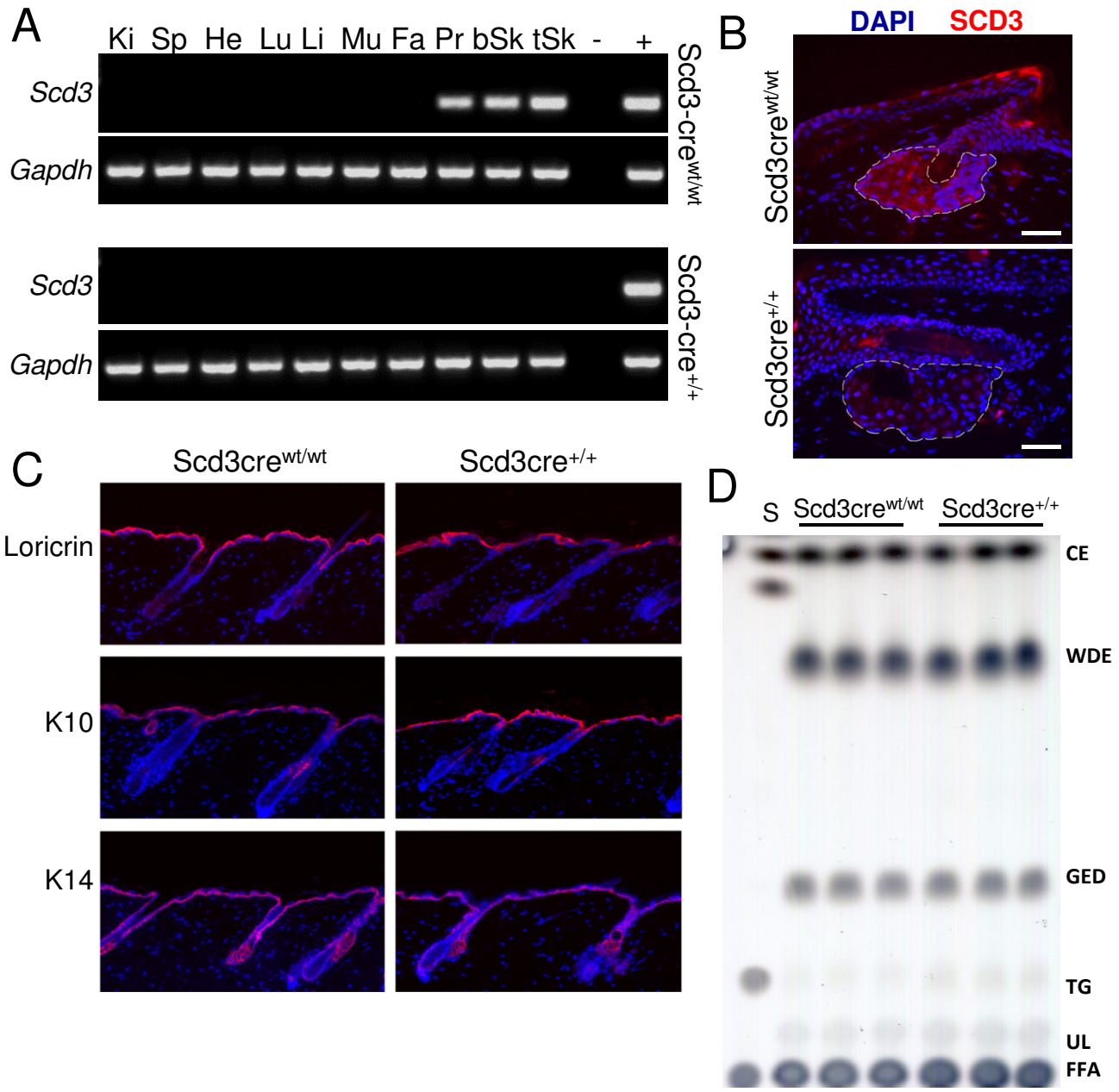

Fig. S2. Lack of SCD3 expression in homozygous Scd3cre mice has no phenotypical consequences. (A) RT-PCR analysis revealed that *Scd3* transcripts were readily detectable in the preputial gland (Pr) and the back (bSk) and tail (tSk) skin of control mice. In contrast, no *Scd3* expression was detectable in Scd3cre$^{+/+}$ animals. Ki, kidney; Sp, spleen; He, heart; Lu, lung; L, liver; Mu, muscle; Fa, fat. (B) Loss of Scd3 protein in Scd3cre$^{+/+}$ animals was confirmed using immunofluorescence. (C) Immunofluorescence revealed no changes in the expression pattern of the epidermal differentiation markers loricrin, K10, and K14 in mice lacking SCD3. (D) Thin layer chromatography revealed no quantitative or qualitative changes in hair lipids of Scd3-deficient mice. S, standard. Scale bars in B represent 100 µm.

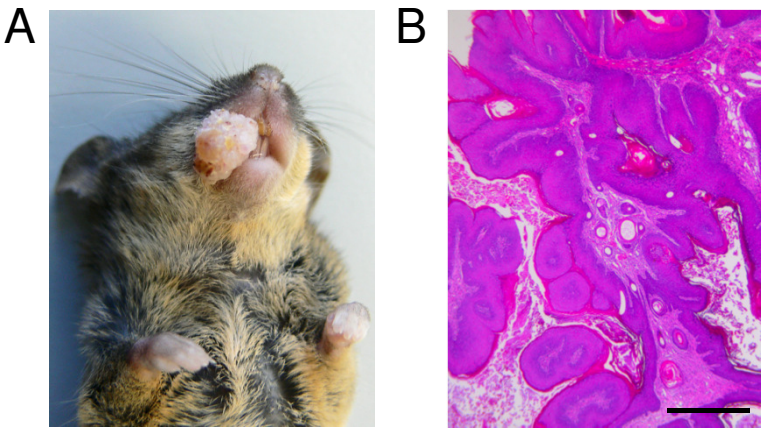

Fig. S3. (A) Representative example of the macroscopical aspect of oral tumors that developed in single Scd3cre$^{+/wt}$+Kras mice. (B) Histological analysis of H&E-stained skin sections of the tumors. Scale bar in B represents 500 µm.

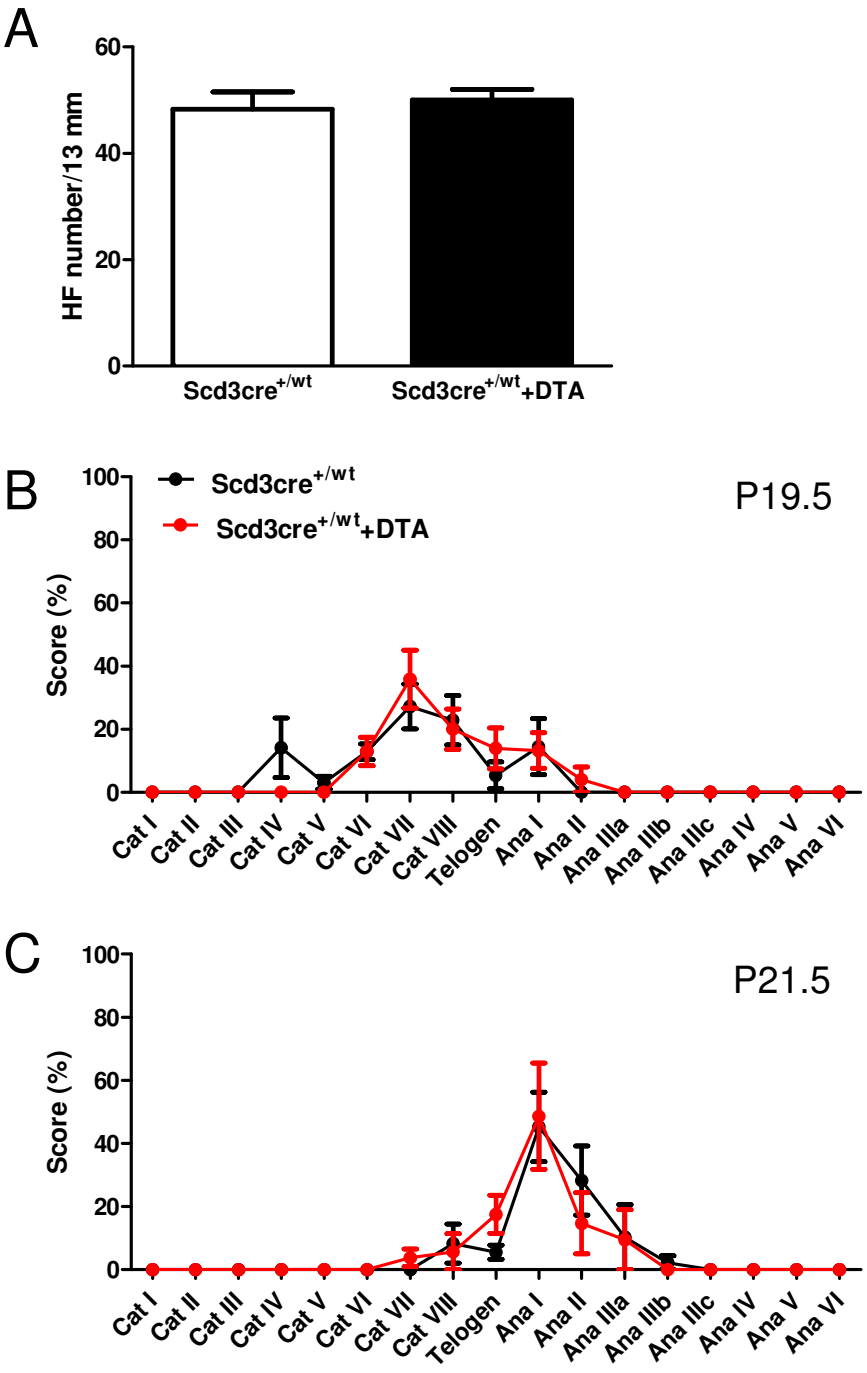

Fig. S4. No changes were observed in the hair follicle density in the back skin of Scd3cre$^{+/wt}$+DTA mice (A). Quantitative hair cycle histomorphometry revealed no significant changes in hair follicle cycling during the examined time points, i.e. around the initiation of hair follicle cycling by the first spontaneous catagen development (day P19.5) (B) and the subsequent first entry into telogen (day P21.5) (C).

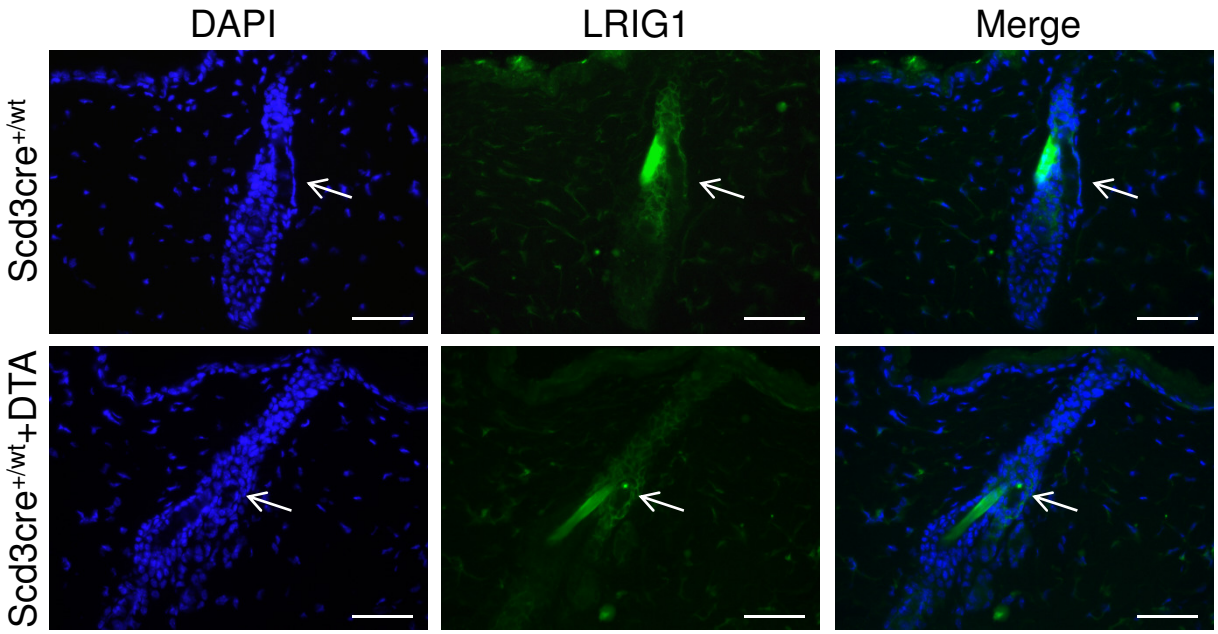

Fig. S5. Immunofluorescence staining revealed that normal LRIG1 expression is maintained in the pilosebaceous unit of Scd3cre$^{+/wt}$+DTA mice. The white arrows indicate the position of the sebaceous gland. Scale bars indicate 50 μm.

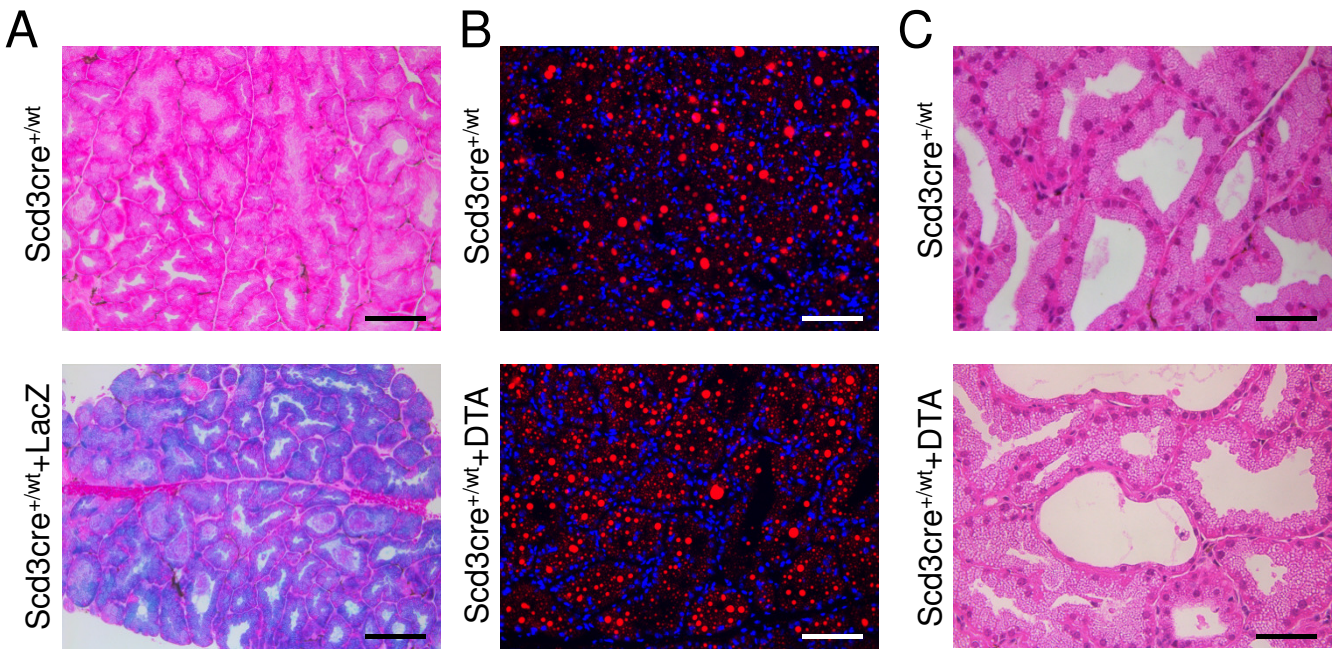

Fig. S6. Expression of cre and analysis of DTA-induced changes in the Harderian gland. (A) Staining for β-galactosidase activity revealed widespread expression of cre in Harderian glands of Scd3cre$^{+/wt}$+LacZ mice (lower panel). (B) Fluorescent images of DAPI and Nile red-stained sections suggests that lipid production is largely maintained in the Harderian glands of Scd3cre$^{+/wt}$+DTA mice. (C) H&E staining showing normal acinar structure in the Harderian gland of control mice (Scd3cre$^{+/wt}$, upper panel). In Harderian glands of Scd3cre$^{+/wt}$+DTA mice (lower panel), multifocal acinar dilatation with epithelial flattening, loss of lipid droplets, and the presence of dark, elongated nuclei was observed. Scale bars indicate 100 µm (A, B) or 50 µm (C).